

Article

Hydroxyapatite–Clay Composite for Bone Tissue Engineering: Effective Utilization of Prawn Exoskeleton Biowaste

Perabathula Satish ¹, Komalakrushna Hadagalli ^{1,2}, Lakkimsetti Lakshmi Praveen ¹, Mahin Saif Nowl ¹, Asif H. Seikh ³, Ibrahim A. Alnaser ^{3,4,*}, Hany S. Abdo ³ and Saumen Mandal ^{1,*}

¹ Department of Metallurgical and Materials Engineering, National Institute of Technology Karnataka (NITK), Surathkal, Mangalore 575025, India; confidence.satish@gmail.com (P.S.); khadaga@g.clemson.edu (K.H.); llpraveen24@gmail.com (L.L.P.); nowlsaif@gmail.com (M.S.N.)

² Department of Materials Science and Engineering, Clemson University, 161 Surrine Hall, Clemson, SC 29634, USA

³ Center of Excellence for Research in Engineering Materials (CEREM), King Saud University, P.O. Box 800, Riyadh 11421, Saudi Arabia; aseikh@ksu.edu.sa (A.H.S.); habdo@ksu.edu.sa (H.S.A.)

⁴ Mechanical Engineering Department, College of Engineering, King Saud University, P.O. Box 800, Riyadh 11421, Saudi Arabia

* Correspondence: ianaser@ksu.edu.sa (I.A.A.); smandal@nitk.edu.in (S.M.)

Abstract: Hydroxyapatite (HA, $\text{Ca}_{10}(\text{PO}_4)_6(\text{OH})_2$)-based porous scaffolds have been widely investigated in the last three decades. HA, with excellent biocompatibility and osteoconductivity, has made this material widely used in bone tissue engineering. To improve the mechano-biological properties of HA, the addition of clay to develop HA-based composite scaffolds has gained considerable interest from researchers. In this study, a cost-effective method to prepare a HA–clay composite was demonstrated via the mechanical mixing method, wherein kaolin was used because of its biocompatibility. Prawn (*Fenneropenaeus indicus*) exoskeleton biowaste was utilized as a raw source to synthesize pure HA using wet chemical synthesis. HA–clay composites were prepared by reinforcing HA with 10, 20, and 30 wt.% of kaolin via the mechanical mixing method. A series of characterization tools such as XRD, FTIR, Raman, and FESEM analysis confirmed the phases and characteristic structural and vibrations bonds along with the morphology of sintered bare HA, HA–kaolin clay composite, and kaolin alone, respectively. The HA–clay composite pellets, uniaxially pressed and sintered at 1100 °C for 2 h, were subjected to a compression test, and an enhancement in mechanical and physical properties, with the highest compressive strength of 35 MPa and a retained open porosity of 33%, was achieved in the HA–kaolin (20 wt.%) clay composite, in comparison with bare HA. The addition of 20% kaolin to HA enhanced its compressive strength by 33.7% and increased its open porosity by 19% when compared with bare HA. The reinforcement of HA with different amounts (10, 20, 30 wt.%) of kaolin could open up a new direction of preparing biocomposite scaffolds with enhanced mechanical properties, improved wear, and better cell proliferation in the field of bone tissue engineering.

Keywords: hydroxyapatite; clay; sintering; composite; compressive strength; porosity



Citation: Satish, P.; Hadagalli, K.; Praveen, L.L.; Nowl, M.S.; Seikh, A.H.; Alnaser, I.A.; Abdo, H.S.; Mandal, S. Hydroxyapatite–Clay Composite for Bone Tissue Engineering: Effective Utilization of Prawn Exoskeleton Biowaste. *Inorganics* **2023**, *11*, 427. <https://doi.org/10.3390/inorganics11110427>

Academic Editors: Vladimir Arion and Wolfgang Linert

Received: 14 September 2023

Revised: 17 October 2023

Accepted: 25 October 2023

Published: 31 October 2023



Copyright: © 2023 by the authors. Licensee MDPI, Basel, Switzerland. This article is an open access article distributed under the terms and conditions of the Creative Commons Attribution (CC BY) license (<https://creativecommons.org/licenses/by/4.0/>).

1. Introduction

Hydroxyapatite (HA, $\text{Ca}_{10}(\text{PO}_4)_6(\text{OH})_2$) is an important bioceramic material which is extensively used in bone tissue engineering due to its chemical composition, which is like that of human bones and teeth [1,2]. It has distinctive biological properties, such as osteoconductive, bioactive, nontoxic, noninflammatory, and biodegradable properties, and has excellent biocompatibility [3]. Since HA strongly bonds to surrounding tissue when implanted in the human body, it has been successfully used for orthopedics and dentistry for the past few decades [4]. However, due to its inadequate mechanical properties, HA is unable to serve as a load-bearing implant [5]. So, the use of HA as a filler for bone defects has been limited to non-load bearing areas and coatings on metallic implants for

their firm fixation with the host bone [6]. Therefore, additives like ZrO_2 , Al_2O_3 , SiC, and metal fibers can be included in order to enhance the mechanical reliability of HA, but they are ruinous to the biological properties of HA. So, the addition of clays has gained considerable attention. As clays are nontoxic, their composites can be used in biomedical applications such as tissue engineering, bone cement, wound healing, drug delivery, and enzyme immobilization [7]. As bone tissue engineering (BTE) is mainly based on the formation of tissues and bone mechanics, scaffolds, cells, and growth factors are the three main components of BTE. The useful characteristics of bones, such as their role in body structure, defense of key internal organs, facilitation of mobility, and storage of calcium and phosphate-based minerals, have increased the significance of bone tissue engineering [8,9]. Additionally, the growing importance of bone tissue engineering has been influenced by the rise in knee and hip replacement procedures over the last few years as well as the drawbacks of existing treatment options such as allografts, autografts, and ceramic and metallic implants [10]. Scaffolds are three-dimensional porous structures which play a crucial role in tissue engineering investigations. Although HA can be used to prepare scaffolds, most BTE studies entail the use of polymers (both synthetic and natural) and fillers for the preparation of composite scaffolds.

Different types of clays, namely montmorillonite (MMT) and kaolin clays, have been reported in the literature to improve the mechanical properties of biocomposite scaffolds [11]. Kaolin is one of the most important clay minerals used in the industry. It comprises majorly kaolinite mineral, which is a hydrated aluminum silicate, $Al_2Si_2O_5(OH)_4$. Kaolinite is also called china clay and it is a layered silicate mineral, with one octahedral sheet of alumina (AlO_6) octahedra attached through oxygen atoms to one tetrahedral sheet of silica (SiO_4) [12]. Kaolinite is earthy, soft, and generally white in color, which is produced via the weathering/chemical oxidation of mineral ores of aluminum silicates. It has low cation exchange capacity (CEC), which lies in the range of 1–15 meq/100 g [13]. Kaolin has found its applications in the paper [14], cement [15], textile [16], paint [17], and rubber industries [18], as well as a catalyst [19] and in ceramics [20] and civil engineering applications [21]. Kaolin can also be used to produce fiberglass [22]. Fiberglass has a number of applications which include insulation, plastics reinforcement, textile yarns, and substrates for electronic circuit boards [23]. Kaolin can be used as a filler in plastics because it helps to produce a better surface finish [24]. Kaolin has certain advantages like high specific surface area and low cost [25]. It has been reported that with the addition of kaolin, scaffolds exhibit a more stable and desirable pH environment and an enhanced protein adsorption capacity [26].

MMT clay with a hydroxyapatite layer can be used as a filler with remineralizing potential in composites for dental applications [27]. To enhance the strength of a HA/polymer composite for bone replacement, MMT can be used as a reinforcing agent. Katti et al. reported that the addition of MMT clay to a HA/chitosan/MMT composite increased the hardness and elastic modulus of the composite [28]. Other studies revealed that the addition of MMT clay to MMT/chitosan/HA- ZrO_2 [29] and MMT/chitosan/HA-ZnO composites improved their tensile strength. Obada et al. reinforced HA with kaolin clay using the sol-gel method to enhance the mechanical and biological properties of bioceramics [26]. The reported mechanical measurement data affirm that reinforced hydroxyapatite scaffolds can serve as an alternative for human trabecular bones, whose compressive strength lies in the range of 2–12 MPa [30]. However, the brittleness and lack of mechanical stability of HA-clay composite scaffolds are some of their significant drawbacks, preventing their application in extensive bone regeneration. The reinforcement of hydroxyapatite with clay could open a new direction of preparing scaffolds with enhanced mechanical properties, improved sinterability leading to high strength with retained porosity, and better cell proliferation in the field of bone tissue engineering.

In the present study, prawn shell exoskeleton biowaste was utilized as a Ca-rich raw source for HA synthesis. Kaolin clay was selected as a reinforcing material to prepare HA-kaolin clay (0, 10, 20, 30 wt.%) composites by the mechanical mixing and uniaxial pressing methods. In order to retain high compressive strength in the HA-clay composite

while retaining high porosity, the sintering scheme and clay addition were optimized. X-ray diffraction (XRD), field emission scanning electron microscopy (FESEM), Raman spectra, and Fourier transform infrared spectroscopy (FTIR) of bare HA, HA–clay composite, and bare kaolin were carried out to analyze the phases present in HA. Differential scanning calorimetry (DSC) and thermogravimetric analysis (TGA) provided an insight into the thermal activity of the HA–clay composite during sintering. To assess mechanical properties, compression strength was determined, and to assess physical properties, bulk and apparent densities and open porosities were estimated by Archimedes' principle.

2. Results and Discussion

2.1. Structural and Vibrational Analysis

The XRD pattern of bare HA, HA–clay composites, and bare kaolin are shown in Figure 1a–e, respectively. The XRD pattern of sintered HA powder is shown in Figure 1a. It can be observed that a major reflection occurs at 31.69° , which matches with pure HA, (reflection ICDD number: 01-074-0565). Other prominent reflections are found at 16.92° , 25.94° , 28.12° , 32.74° , and 34.1° . The XRD patterns of the HA–clay composites show kaolin peaks at 21.68° in addition to HA peaks, which are shown in Figure 1b–d. In Figure 1e, the XRD pattern of kaolin shows two notable reflections at 12.36° and 24.89° , which match with Bragg's reflections (ICDD 01-089-6538). A series of peaks is found at 19.9° , 20.34° , 21.26° , 35.97° , 38.44° which confirms the phase purity of kaolin powder. Figure 1b–d show peaks around 21.35° along with other series of peaks which confirm the formation of a HA–clay composite. However, major reflections of kaolin at 12.36° and 24.89° are absent in the HA–clay composites due to phase transformations that occur during the sintering process [31]. These phase transformations can be clearly analyzed from the DSC thermal analysis performed on kaolin.

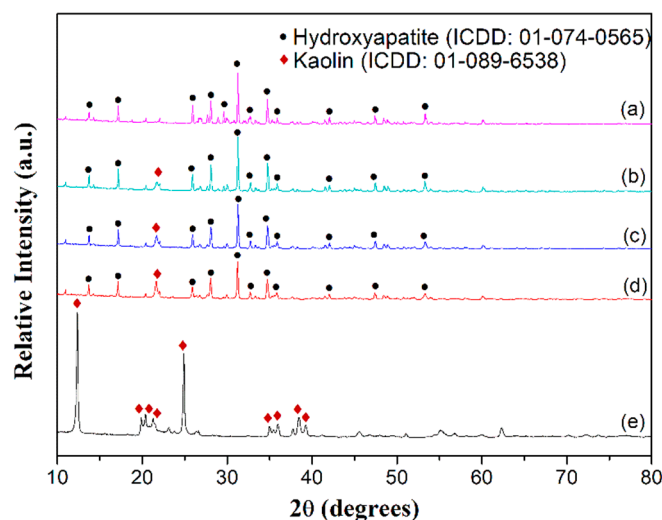


Figure 1. XRD pattern of (a) sintered HA; (b) 90% HA + 10% kaolin; (c) 80% HA + 20% kaolin; (d) 70% HA + 30% kaolin; (e) kaolin.

The FTIR spectra of HA, kaolin, and HA–clay composites with different wt. % kaolin are shown in Figure 2. In Figure 2a, the FTIR spectrum of HA reveals characteristic peaks around wavenumbers 563 , 597 , 724 , 966 , 1027 and 1098 cm^{-1} due to the presence of a PO_4^{3-} group in HA [32]. IR bands at 563 , 597 , and 724 cm^{-1} are due to phosphate bending vibrations, and those at 966 , 1027 , and 1098 cm^{-1} are due to phosphate stretching vibrations. A weaker peak at 1540 cm^{-1} is due to traces of carbonate ions, which are due to environmental reactions with atmospheric CO_2 . Another broad peak found at 3426 cm^{-1} corresponds with the stretching of the structural OH^- band [33]. Likewise, asymmetric stretching and asymmetric bending modes are observed for the phosphate and carbonyl

groups [32]. Figure 2b–d show the similar characteristic peaks of HA where the amount of kaolin varies from 10 to 30 wt%. In accordance with the stretching frequencies of OH groups, kaolin possesses absorption bands between 3500 and 3700 cm^{-1} , as shown in Figure 2e. The FTIR spectrum of kaolin reveals the presence of two bands at 3688 and 3614 cm^{-1} due to stretching vibrations of the O–H bond [34]. The bands observed at 1117, 1025, and 1005 cm^{-1} in pure kaolin are attributed to Si–O stretching vibration [34]. An Al–OH absorption peak is revealed at 910 cm^{-1} [35]. The bands located at 792 and 751 cm^{-1} are assigned to vibrations of the Si–O–Al groups [34]. The band located at 675 cm^{-1} is attributed to the vibration of the Al–OH group [34]. The band located at 560 cm^{-1} corresponds to the vibration of the Si–O–Al group. The kaolin structure is chaotic and easier to dehydrate when the band at 3688 cm^{-1} vanishes. Figure 2b–d show peaks around 1117, 1025, and 563 cm^{-1} , which confirm the presence of kaolin in the HA–clay composite [36]. The assigned vibrational bands from the FTIR spectrum are shown in Table 1.

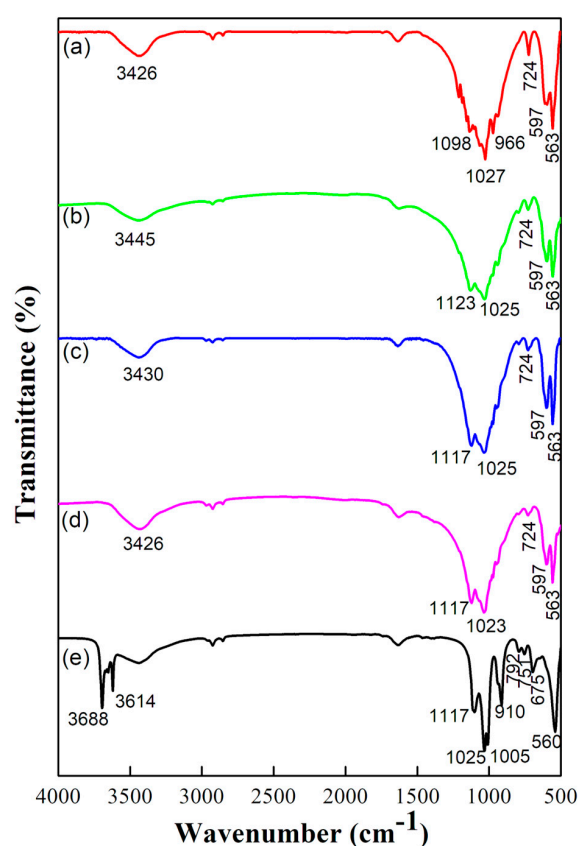


Figure 2. FTIR spectra of (a) sintered HA; (b) 90% HA + 10% kaolin; (c) 80% HA + 20% kaolin; (d) 70% HA + 30% kaolin; (e) kaolin.

Table 1. Vibration modes in FTIR spectrum of HA–clay composite.

Wavenumber (cm^{-1})	Stretching Mode	Functional Group	Source
560, 751, 792	-	Si–O–Al	Kaolin
563, 597, 724	Asymmetric bending	PO_4^{3-}	HA
966	Symmetric stretching	PO_4^{3-}	HA
1023–1027, 1098	Asymmetric stretching	PO_4^{3-}	HA
675, 910	-	Al–OH	Kaolin
1005, 1025	In-plane stretching	Si–O	Kaolin
1117–1123	Longitudinal mode	Si–O	Kaolin
1540	Asymmetric stretching	CO_3^{2-}	Atmospheric CO_2
3426	Stretching of OH–	OH^-	HA

Figure 3a–d shows the Raman spectra of HA and HA composites with 10, 20, and 30 wt% of kaolin clay, respectively; the peak vibrational mode summary is tabulated in Table 2. The band at 972 cm^{-1} corresponds to the ν_1 (stretching mode) symmetric vibrational mode of P–O. The bands located near 412 cm^{-1} and 737 cm^{-1} were the ν_2 (doubly bending mode) and ν_4 (triply degenerate bending mode) PO_4 vibrational modes. The ν_3 (triply generate antisymmetric stretching mode) vibrational mode of PO_4 was located at 1045 cm^{-1} [37]. The peaks at 620 cm^{-1} for the 80% HA + 20% kaolin composite and 615 cm^{-1} for the 70% HA + 30% kaolin composite are due to the translation of the Si–O–Al group in the kaolin of HA–clay composites [38]. Figure 3e shows the Raman spectra of kaolin where peak intensities could only be observed under an enlarged view (inset of Figure 3). The bands at 3696 cm^{-1} and 3620 cm^{-1} correspond to the ν_1 and ν_5 stretching modes of the inner surface hydroxyl groups [39,40]. These bands are further present in all HA–clay composites, which is represented by the shaded area.

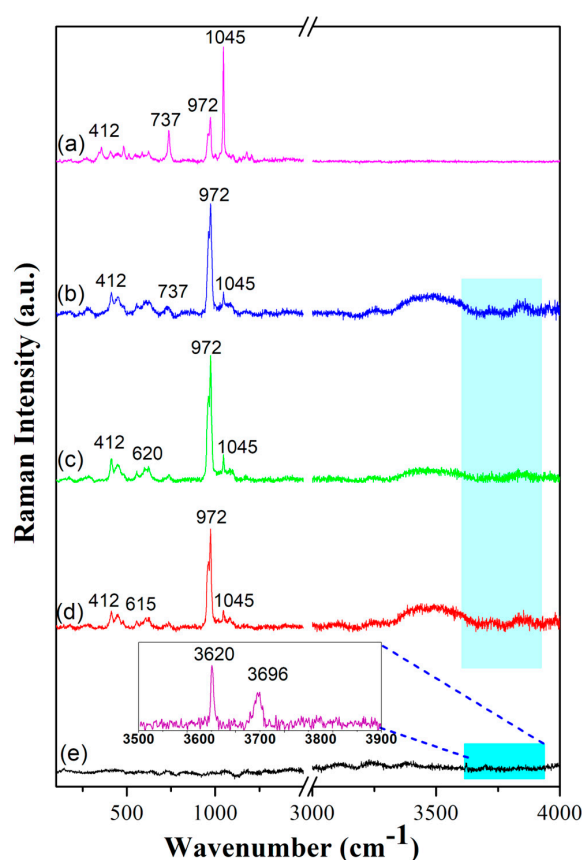


Figure 3. Raman spectra of (a) sintered HA; (b) 90% HA + 10% kaolin; (c) 80% HA + 20% kaolin; (d) 70% HA + 30% kaolin; (e) kaolin.

Table 2. Vibration modes in Raman spectra of HA–clay composites.

Wavenumber (cm^{-1})	Assignment	Vibration Groups	Source
972	Symmetric vibrational mode of P–O (stretching mode)	$\nu_1 \text{ PO}_4^{3-}$	HA
412	Doubly bending mode	$\nu_2 \text{ PO}_4^{3-}$	HA
1045	Triply generate antisymmetric stretching mode	$\nu_3 \text{ PO}_4^{3-}$	HA
737	Triply degenerate bending mode	$\nu_4 \text{ PO}_4^{3-}$	HA
615–620	Si–O–Al translation	Si–O–Al	Kaolin
3620	O–H stretching	$\nu_5 \text{ OH}^-$	Kaolin
3696	O–H stretching	$\nu_1 \text{ OH}^-$	Kaolin

2.2. Thermal Analysis

Figure 4a–e represent the DSC analysis of pure HA, kaolin, and HA with various weight proportions of kaolin, respectively. In pure HA, the endothermic peak at 80 °C corresponds to the removal of adsorbed water from the lattice. It is reported that heating apatite at higher temperatures can lead to dehydroxylation, which is reflected in the exothermic peak of pure HA at 715 °C [41]. Similarly, Skinner et al. reported that the dehydroxylation of HA starts above 700 °C [42]. The endothermic peak at 498 °C corresponds to the dehydroxylation of kaolinite, which is reflected in kaolin and the HA–kaolin composites [40,43]. Here, dehydroxylation of the crystalline kaolinite structure took place, resulting in the formation of a calcined metakaolin phase. Also, the exothermic peak at 718 °C in Figure 4c shows the dehydroxylation of HA, and exothermicity tends to diminish with the increased addition of kaolin to 20% and 30%, with a slight shift in the dehydroxylation temperature.

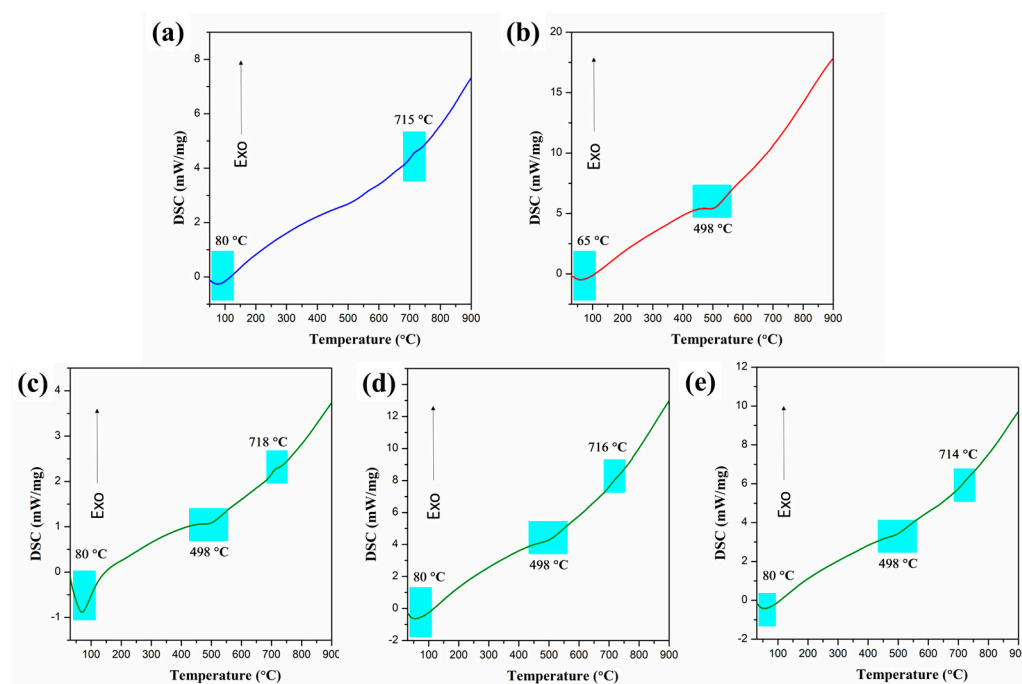


Figure 4. DSC analysis of (a) pure HA; (b) kaolin; (c) 90% HA + 10% kaolin; (d) 80% HA + 20% kaolin; (e) 70% HA + 30% kaolin.

The thermal behavior of pure HA along with that of kaolin and blended HA (10 wt %, 20 wt%, 30 wt% kaolin) was studied by thermogravimetric analysis (TGA). The percentage weight loss of pure HA, kaolin, and HA with various weight percentages of kaolin is represented in Figure 5a–e, respectively. The weight loss that occurred around 210 °C and 420 °C could be attributed to the dehydration and dehydroxylation of adsorbed water, expelled from the mineral lattice of kaolin. A total of 14% weight loss was observed in pure HA. Through the interpolation of TG curves, the percentage weight loss of kaolinite mineral in HA with 10 wt % kaolin was found to be around 8%. The corresponding TGA peak between 515 °C and 750 °C is a clear indication of weight loss occurring due to the dehydroxylation of kaolinite clay mineral within the composite [44].

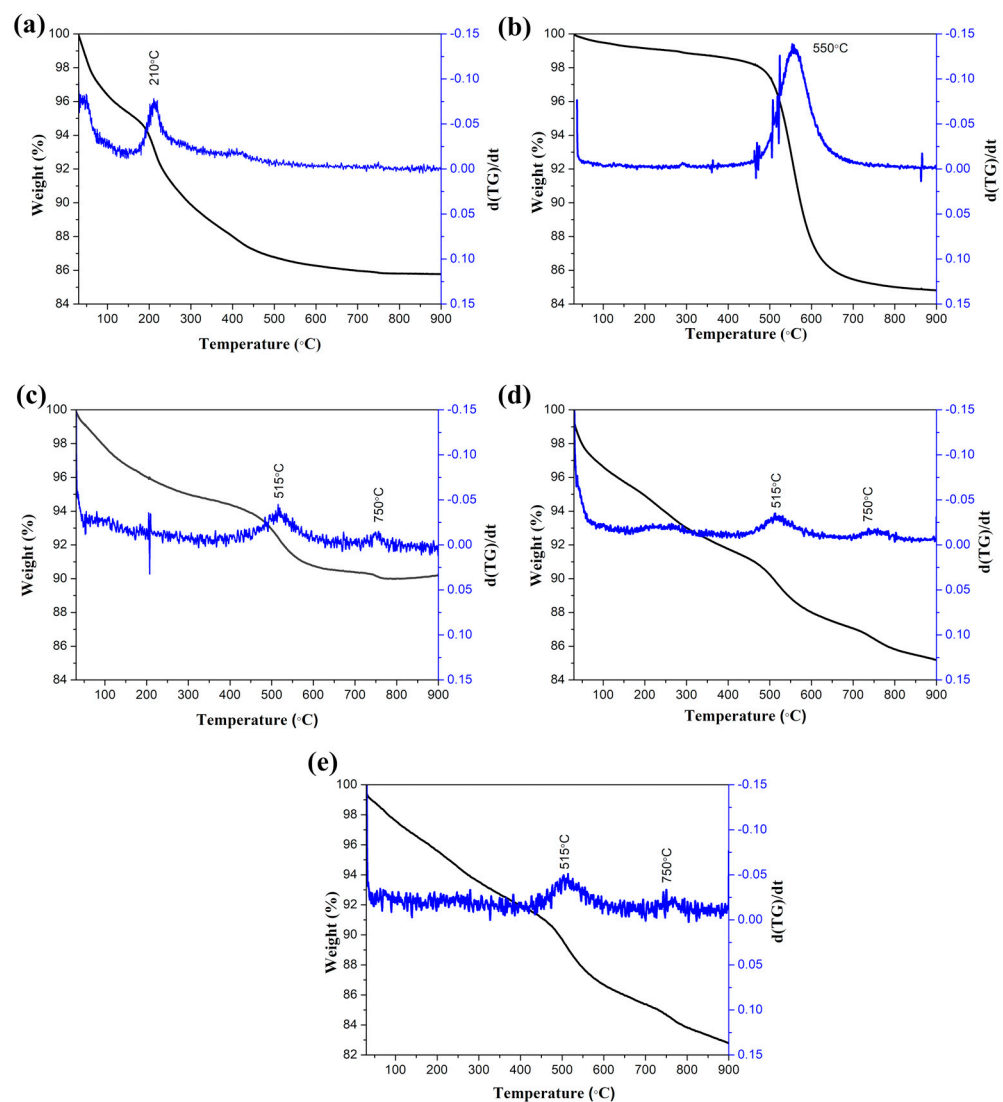


Figure 5. Thermogravimetric analysis of (a) pure HA; (b) kaolin; (c) 90% HA + 10% kaolin; (d) 80% HA + 20% kaolin; (e) 70% HA + 30% kaolin.

2.3. Morphological Analysis

Morphological analyses conducted using FESEM on sintered HA, kaolin, and HA clay composites, and the corresponding images are shown in Figure 6a, 6b, 6c, 6d, and 6e, respectively. A dense morphology and well-sintered uniaxial grains were observed in sintered HA, as shown in Figure 6a. A flake-like morphology [45] and more agglomeration was observed in pure kaolin clay, as shown in Figure 6b. Figure 6c–e show micrographs of HA–clay composites with the addition of kaolin (10, 20, 30 wt %) which were sintered at 1100 °C for 2 h. It is observed that the flake-like structures of kaolin clay were reinforced with HA, creating porosities within the nanocomposite and leading to a flocculating morphology, as shown in Figure 6c–e [46].

Energy-dispersive X-ray spectroscopy (EDS) was conducted on prawn-shell-derived HA; the results are shown in Figure 7. The EDS spectrum revealed the presence of calcium, phosphorus, oxygen, and various other trace elements like Mg, Na, Si, and Fe. The weight percentages of Ca and P were obtained as 40.59% and 24.6%. The ratio of HA obtained from these was 1.65. The weight percentages of other trace elements like Mg, Na, Si, and Fe, which help in rapid bone regeneration [47], were obtained as 2.41%, 0.8%, 0.44%, and 0.6%.

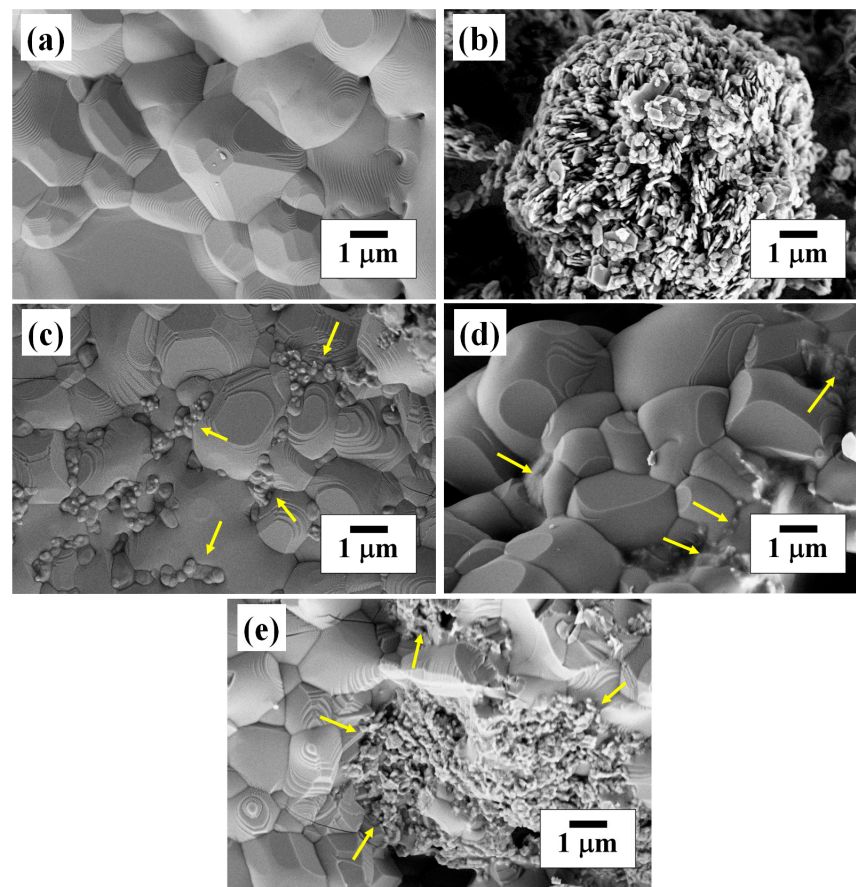


Figure 6. Microstructure of (a) sintered HA; (b) kaolin; (c) 90% HA + 10% kaolin; (d) 80% HA + 20% kaolin; (e) 70% HA + 30% kaolin. (Yellow arrows represent the presence of kaolin.)

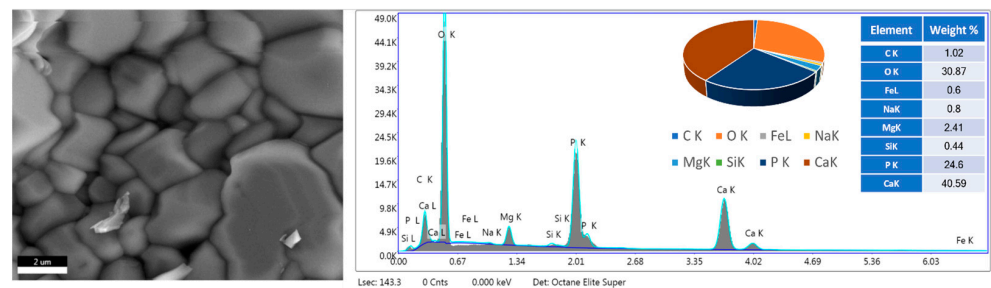


Figure 7. Energy-dispersive X-ray spectroscopic analysis of sintered HA.

2.4. Mechanical and Physical Properties

With reference to mechanical properties, Figure 8A shows the stress–strain curves of sintered HA (Figure 8A(a)) and various (10–30 wt.%) HA–clay composites (Figure 8A(b–d)). It can be observed that bare HA exhibited a compressive strength of 26 ± 1.2 MPa, whereas the addition of a clay component in 90% HA + 10% kaolin and 80% HA + 20% kaolin produced an increase in compressive strength from 30 ± 2.8 MPa to 34.76 ± 6.7 MPa. Further addition of kaolin in 70% HA + 30% kaolin produced a decrease in compressive strength to 33 ± 0.4 MPa, as shown in Figure 8B. It was found that an increment in the mechanical properties of HA occurs with the addition up to 20 wt % of kaolin; then, further addition leads to a decline in strength [48]. Obada et al. reported the compressive strengths of HA–kaolin clay composites (15 wt% of kaolin) under various sintering temperatures. At 900, 1000, and 1100 °C, compressive strengths were found to be 5.67, 6.33, and 7.66 MPa, which is a lot lower compared with the present results [26]. Scaffolds should have high

mechanical strength, as the cortical bone has an elastic modulus in the range of 1–20 GPa and a compressive strength of 1–100 MPa; but the mechanical properties of sintered scaffolds are comparable to those of the cancellous bone, which has an elastic modulus of 0.1 to 1.0 GPa and a compressive strength of 1–10 MPa [49]. The addition of clay led to an increment in compressive strength, which may have been due to the impact of reinforcement, although there was decrease in apparent density. This decrement in density could have been due to the flake morphology of the clay, which marginally filled most of the pores [26].

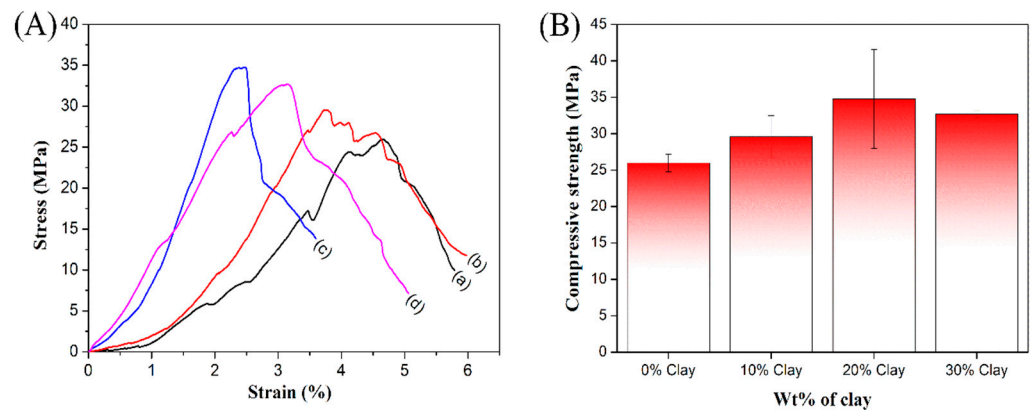


Figure 8. (A) Stress–strain curves of sintered specimens of (a) sintered HA; (b) 90% HA + 10% kaolin; (c) 80% HA + 20% kaolin; (d) 70% HA + 30% kaolin. (B) Variation in compressive strength with different wt % of clay.

The physical properties of HA–clay composites were determined by open porosities which originate from the escape of a small amount of water from kaolin during sintering. Figure 9a shows the variation in apparent density and bulk density, with different weight percentages (0, 10, 20, 30) of kaolin clay added to HA. Figure 9b shows the variation in open porosity with different weight % of kaolin clay. The bulk and apparent densities of bare HA, 90% HA + 10% kaolin, 80% HA + 20% kaolin, and 70% HA + 30% kaolin clay composites were found to be 2.34 g/cc, 1.75 g/cc, 1.66 g/cc, and 1.71 g/cc and 2.67 g/cc, 2.47 g/cc, 2.22 g/cc, and 2.22 g/cc, respectively. The open porosity of bare HA was found to be 14%. But in the case of HA–clay composites, it was observed that open porosity increased up to 33% with the addition of 20 wt.% kaolin and further decreased to 29% with the addition of 30 wt.% kaolin [50]. This was because of several possible reasons, like the dehydroxylation of kaolinite mineral and the complex interaction pattern between hydroxyapatite and clay. The present work focuses on the effect of adding kaolin to pure hydroxyapatite (HA) which was derived from prawn shell biowaste to achieve high mechanical strength with retained porosity.

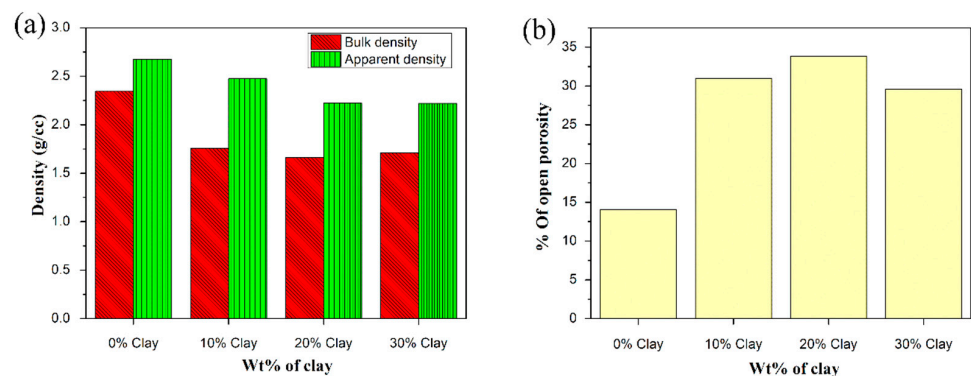


Figure 9. Variation in physical properties of HA–kaolin clay composites with different wt.% (0, 10, 20, and 30) of added kaolin clay; (a) bulk and apparent densities; (b) open porosity.

3. Materials and Methods

3.1. Materials

Prawn shell (*Fenneropenaeus indicus*) waste was collected from a local fish market and the shells were separated. Prawn exoskeleton is a source of calcium carbonate. Prawn shells were thoroughly washed with tap water and hot distilled water. After being washed, the prawn shells were dried for six hours in an oven at 150 °C before being pulverized. Kaolin (200 mesh) was purchased from Molychem chemicals (Mumbai, India).

3.2. Preparation of Hydroxyapatite Clay Composite from Prawn Shells

The wet chemical synthesis method was employed to prepare hydroxyapatite using prawn-shell-derived CaO and orthophosphoric acid. The procedure used to obtain HA–clay composite is shown in Figure 10.

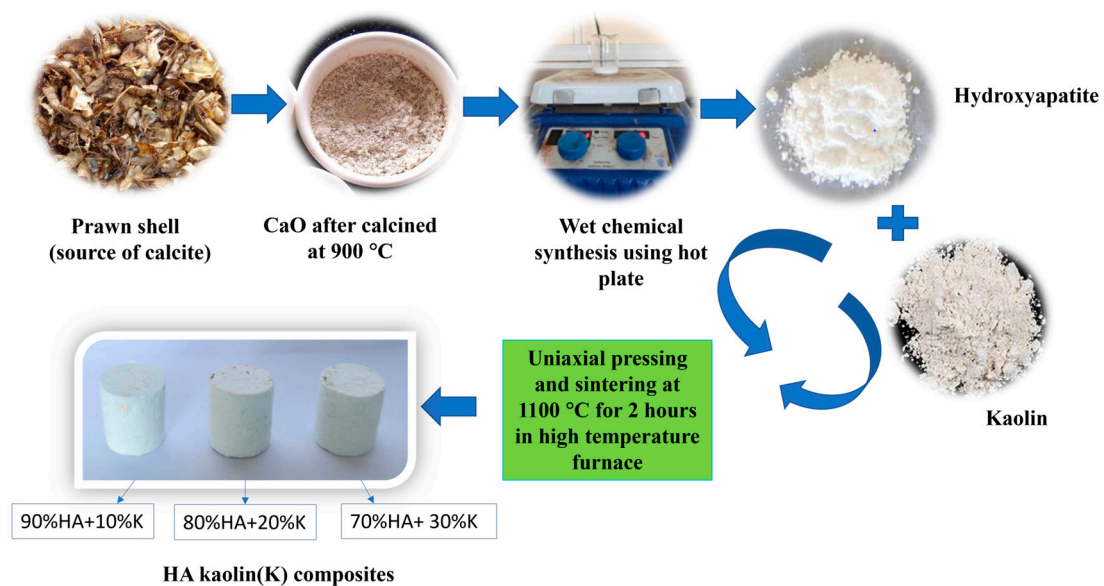


Figure 10. Process flow diagram of HA–clay composite preparation.

Powdered prawn shell, which contains calcite, was subjected to calcination in a muffle furnace at 900 °C for 12 h. Prawn shell exoskeleton comprises calcite, proteins, and α -chitin [33], with calcite forming the majority. The prawn shells were calcined to remove unwanted carbonaceous material and organic matter, leaving behind pure CaO. Calcite is converted into calcium oxide by emitting carbon dioxide. The main advantage of using prawn-shell-derived calcium oxide is the existence of trace elements like Mg, Na, and Fe, which aid in faster bone regeneration [51].

Using the wet chemical synthesis approach, CaO was added to distilled water, followed by gradual dropwise addition of orthophosphoric acid (H_3PO_4) to maintain a Ca/P molar stoichiometric ratio of 1.66 [52]. Ammonia solution was added dropwise during the experiment to keep the pH level at 10. A hot plate with a magnetic stirrer was used to conduct this reaction for 48 h at room temperature and 200 rpm in a closed container. Subsequently, the resultant precipitate obtained from the reaction was dried overnight at 100 °C in a hot air oven to produce HA. Then, the HA powder and different wt.% (10, 20, and 30) of kaolin clay were mechanically mixed using agate mortar and pestle and the resulting powder was subjected to uniaxial pressing to obtain green pellets with a compressive load of 12.5 kN. The green pellets were sintered in air at 1100 °C for 2 h in a programmable high-temperature furnace (Nabertherm, Bremen, Germany), resulting in HA–kaolin clay composites.

3.3. Characterization Tools

To determine the phases present in the synthesized powders, X-ray diffractometer (Empyrean, Malvern PANalytical, Netherlands) with Cu K α radiation at a scan rate of 2 °/min was used. Field emission scanning electron microscopy (FESEM 7610FPLUS, Jeol, Japan) with an accelerating voltage of 5 kV was utilized to determine the microstructure of the sintered HA–clay composites. Fourier transform infrared spectroscopy (Alpha II, Bruker, Germany) was used to detect the functional groups present in the samples. FTIR spectra were taken at an average scan rate of 24 scans and 4 cm^{−1} resolution in a wavenumber range of 550–4000 cm^{−1}. Raman spectroscopy (Renishaw, UK) was used to determine the vibrational states and characteristic bonds in the samples. Raman spectra were taken in a wavenumber range of 100–3000 cm^{−1}. Weight loss changes were observed in the samples within a temperature range of 20 °C–900 °C, at a constant heating rate of 10 °C/min using a thermogravimetric analyzer (PerkinElmer, Singapore). Differential scanning calorimetry (DSC, Netzsch 404 F1, Germany) was carried out to detect exothermic and endothermic transitions at a constant heating rate of 10 °C/min in a temperature range of 30–950 °C. Compressive strength was measured for sintered HA–clay composite specimens using a universal testing machine (UTM, Shimadzu, Japan). Physical properties like apparent density, bulk density, and open porosity of sintered HA–clay composite specimens were measured using a density measurement kit (CAS 44, Contech) by Archimedes' principle method as per ASTM-C373-88 standard. Bulk density, apparent density, and % open porosities were calculated by estimating soaked and dry weights of sintered specimens.

4. Conclusions

The utilization of prawn shell (*Fenneropenaeus indicus*) exoskeleton biowaste as a Ca-rich raw source for HA synthesis was conducted via the wet chemical route. Further, HA–kaolin clay (10, 20, 30 wt.%) composites were developed by the mechanical mixing method. From prominent reflections visible on XRD, the presence of HA and kaolin within the composite was confirmed. FTIR analysis showed that characteristic peaks around 1117, 1025, and 560 cm^{−1} confirmed the presence of kaolin in the HA–clay composites. Characteristic peaks ranging from 615 to 620 cm^{−1} visible in Raman spectra of the HA–clay composites indicated the translation of the Si–O–Al group in kaolin. DSC and TGA analyses of the HA–clay composites revealed their thermal stability, and the endothermic peak at 498 °C corresponded to the dehydroxylation of kaolinite. Dense and flocculating morphologies were observed in FESEM of the sintered HA and HA–clay composites, respectively, whereas flake morphology was observed in kaolin. Uniaxially pressed HA–clay composite specimens were sintered in air at 1100 °C for 2 h to determine their physical and mechanical properties. The addition of 20% kaolin to HA enhanced its compressive strength by 33.7% in comparison to bare HA. The increase in open porosity with the addition of kaolin caused a ~10% decrease in apparent density. It was observed that there was an increment in compressive strength, although there was a considerable increase in open porosity. This improved the mechanical properties of the HA–clay composites, making this class of material a promising alternative material in bone tissue engineering, aimed at trabecular bone repair and regeneration. Further attempts could be made to investigate biodegradation and biocompatibility by conducting in vitro and in vivo studies.

Author Contributions: Conceptualization, P.S., K.H., L.L.P., M.S.N., A.H.S., I.A.A., H.S.A. and S.M.; Methodology, P.S., K.H., L.L.P. and M.S.N.; Software, A.H.S. and S.M.; Validation, I.A.A., H.S.A. and S.M.; Formal Analysis, P.S. and K.H.; Investigation, P.S., K.H., L.L.P., M.S.N., A.H.S., I.A.A., H.S.A. and S.M.; Resources, I.A.A. and S.M.; Data Curation, A.H.S.; Writing—Original Draft Preparation, P.S., K.H. and S.M.; Writing—Review & Editing, H.S.A.; Visualization, P.S., K.H., L.L.P., M.S.N., A.H.S., I.A.A., H.S.A. and S.M.; Supervision, S.M.; Project Administration, A.H.S.; Funding Acquisition, I.A.A. All authors have read and agreed to the published version of the manuscript.

Funding: This work was funded by the Deputyship for Research and Innovation—Ministry of Education in Saudi Arabia for funding this research work through the project no. (IFKSUOR3-323-1).

Data Availability Statement: The data presented in this study are available on a reasonable request from the corresponding authors.

Acknowledgments: This work is supported by the Science and Engineering Research Board (SERB), Department of Science and Technology (CRG/2021/001084). The authors would like to thank the Department of Metallurgical and Materials Engineering, National Institute of Technology, Karnataka, Surathkal, India, for providing laboratory facilities. The authors extend their appreciation to the Deputyship for Research and Innovation, Ministry of Education in Saudi Arabia for funding this research work through the project no. (IFKSUOR3–323–1).

Conflicts of Interest: The authors declare no conflict of interest.

References

1. Satish, P.; Salian, A.; Hadagalli, K.; Mandal, S. Preparation and Structural Characteristics of Biphasic Calcium Phosphates from Prawn Shell Bio-Waste. *Adv. Appl. Ceram.* **2023**, *122*, 69–78. [CrossRef]
2. Bogdanoviciene, I.; Beganskiene, A.; Tönsuaadu, K.; Glaser, J.; Meyer, H.J.; Kareiva, A. Calcium Hydroxyapatite, $\text{Ca}_{10}(\text{PO}_4)_6(\text{OH})_2$ Ceramics Prepared by Aqueous Sol–Gel Processing. *Mater. Res. Bull.* **2006**, *41*, 1754–1762. [CrossRef]
3. Yuan, X.; Xu, Y.; Lu, T.; He, F.; Zhang, L.; He, Q.; Ye, J. Enhancing the Bioactivity of Hydroxyapatite Bioceramic via Encapsulating with Silica-Based Bioactive Glass Sol. *J. Mech. Behav. Biomed. Mater.* **2022**, *128*, 105104. [CrossRef]
4. Venkatesan, J.; Anil, S. Hydroxyapatite Derived from Marine Resources and Their Potential Biomedical Applications. *Biotechnol. Bioprocess. Eng.* **2021**, *26*, 312–324. [CrossRef]
5. Prakasam, M.; Locs, J.; Salma-Ancane, K.; Loca, D.; Largeteau, A.; Berzina-Cimdina, L. Biodegradable Materials and Metallic Implants—A Review. *J. Funct. Biomater.* **2017**, *8*, 44. [CrossRef] [PubMed]
6. Bikramjit Basu Biomaterials Science and Tissue Engineering: Principles and Methods. Available online: <https://www.amazon.com/Biomaterials-Science-Tissue-Engineering-Principles/dp/1108415156> (accessed on 20 October 2023).
7. Sandomierski, M.; Zielińska, M.; Adamska, K.; Patalas, A.; Voelkel, A. Calcium Montmorillonite as a Potential Carrier in the Release of Bisphosphonates. *N. J. Chem.* **2022**, *46*, 3401–3408. [CrossRef]
8. Murugan, R.; Ramakrishna, S. Development of Nanocomposites for Bone Grafting. *Compos. Sci. Technol.* **2005**, *65*, 2385–2406. [CrossRef]
9. Dorozhkin, S.V. Calcium Orthophosphates. *Biomater* **2011**, *1*, 121–164. [CrossRef]
10. Salgado, A.J.; Coutinho, O.P.; Reis, R.L. Bone Tissue Engineering: State of the Art and Future Trends. *Macromol. Biosci.* **2004**, *4*, 743–765. [CrossRef]
11. Kwaśniewska, A.; Chocyk, D.; Gładyszewski, G.; Borc, J.; Świetlicki, M.; Gładyszewska, B. The Influence of Kaolin Clay on the Mechanical Properties and Structure of Thermoplastic Starch Films. *Polymers* **2020**, *12*, 73. [CrossRef]
12. Frost, R.L.; Kristof, J. Raman and Infrared Spectroscopic Studies of Kaolinite Surfaces Modified by Intercalation. In *Clay Surfaces-Fundamental and Applications*; Elsevier: Amsterdam, The Netherlands, 2004; pp. 184–215.
13. Torres-Luna, J.A.; Carriazo, J.G. Porous Aluminosilicic Solids Obtained by Thermal-Acid Modification of a Commercial Kaolinite-Type Natural Clay. *Solid State Sci.* **2019**, *88*, 29–35. [CrossRef]
14. Tunç, S.; Duman, O.; Polat, T.G. Effects of Montmorillonite on Properties of Methyl Cellulose/Carvacrol Based Active Antimicrobial Nanocomposites. *Carbohydr. Polym.* **2016**, *150*, 259–268. [CrossRef]
15. Lemma, R.; Irassar, E.F.; Rahhal, V. Calcined Illitic Clays as Portland Cement Replacements. In *Calcined Clays for Sustainable Concrete*; Springer: Dordrecht, The Netherlands, 2015; pp. 269–276.
16. Elmoubarki, R.; Mahjoubi, F.Z.; Tounsadi, H.; Moustadraf, J.; Abdennouri, M.; Zouhri, A.; El Albani, A.; Barka, N. Adsorption of Textile Dyes on Raw and Decanted Moroccan Clays: Kinetics, Equilibrium and Thermodynamics. *Water Resour. Ind.* **2015**, *9*, 16–29. [CrossRef]
17. Murray, H.H. Overview—Clay Mineral Applications. *Appl. Clay Sci.* **1991**, *5*, 379–395. [CrossRef]
18. Nasruddin; Agustini, S.; Sholeh, M. Utilization of Kaolin as a Filling Material for Rubber Solid Tire Compounds for Two-Wheeled Electric Scooters. *IOP Conf. Ser. Mater. Sci. Eng.* **2021**, *1143*, 012010. [CrossRef]
19. Luo, W.; Fan, Z.; Wan, J.; Hu, Q.; Dong, H.; Zhang, X.; Zhou, Z. Study on the Reusability of Kaolin as Catalysts for Catalytic Pyrolysis of Low-Density Polyethylene. *Fuel* **2021**, *302*, 121164. [CrossRef]
20. Dondi, M.; Iglesias, C.; Dominguez, E.; Guarini, G.; Raimondo, M. The Effect of Kaolin Properties on Their Behaviour in Ceramic Processing as Illustrated by a Range of Kaolins from the Santa Cruz and Chubut Provinces, Patagonia (Argentina). *Appl. Clay Sci.* **2008**, *40*, 143–158. [CrossRef]
21. Abdullah, M.E.; Jaya, R.P.; Shahafuddin, M.N.A.; Yaacob, H.; Wan Ibrahim, M.H.; Nazri, F.M.; Ramli, N.I.; Mohammed, A.A. Performance of Kaolin Clay on the Concrete Pavement. *IOP Conf. Ser. Mater. Sci. Eng.* **2018**, *358*, 012049. [CrossRef]
22. Murray, H.H. Traditional and New Applications for Kaolin, Smectite, and Palygorskite: A General Overview. *Appl. Clay Sci.* **2000**, *17*, 207–221. [CrossRef]
23. Marsh, G. Electronics—A Major Market for Reinforced Plastics. *Reinf. Plast.* **2008**, *52*, 38–41. [CrossRef]
24. Mareri, P.; Bastide, S.; Binda, N.; Crespy, A. Mechanical Behaviour of Polypropylene Composites Containing Fine Mineral Filler: Effect of Filler Surface Treatment. *Compos. Sci. Technol.* **1998**, *58*, 747–752. [CrossRef]

25. Song, S.; Dong, L.; Zhang, Y.; Chen, S.; Li, Q.; Guo, Y.; Deng, S.; Si, S.; Xiong, C. Lauric Acid/Intercalated Kaolinite as Form-Stable Phase Change Material for Thermal Energy Storage. *Energy* **2014**, *76*, 385–389. [[CrossRef](#)]
26. Obada, D.O.; Oseni, S.A.; Sina, H.; Salami, K.A.; Oyediji, A.N.; Dodoo-Arhin, D.; Bansod, N.D.; Csaki, S.; Atta, A.Y.; Fasanya, O.O.; et al. Fabrication of Novel Kaolin-Reinforced Hydroxyapatite Scaffolds with Robust Compressive Strengths for Bone Regeneration. *Appl. Clay Sci.* **2021**, *215*, 106298. [[CrossRef](#)]
27. Sandomierski, M.; Buchwald, Z.; Voelkel, A. Calcium Montmorillonite and Montmorillonite with Hydroxyapatite Layer as Fillers in Dental Composites with Remineralizing Potential. *Appl. Clay Sci.* **2020**, *198*, 105822. [[CrossRef](#)]
28. Katti, K.S.; Katti, D.R.; Dash, R. Synthesis and Characterization of a Novel Chitosan/Montmorillonite/Hydroxyapatite Nanocomposite for Bone Tissue Engineering. *Biomed. Mater.* **2008**, *3*, 034122. [[CrossRef](#)]
29. Bhowmick, A.; Jana, P.; Pramanik, N.; Mitra, T.; Banerjee, S.L.; Gnanamani, A.; Das, M.; Kundu, P.P. Multifunctional Zirconium Oxide Doped Chitosan Based Hybrid Nanocomposites as Bone Tissue Engineering Materials. *Carbohydr. Polym.* **2016**, *151*, 879–888. [[CrossRef](#)]
30. Morgan, E.F.; Unnikrisnan, G.U.; Hussein, A.I. Bone Mechanical Properties in Healthy and Diseased States. *Annu. Rev. Biomed. Eng.* **2018**, *20*, 119–143. [[CrossRef](#)] [[PubMed](#)]
31. Kłosek-Wawrzyn, E.; Małolepszy, J.; Murzyn, P. Sintering Behavior of Kaolin with Calcite. *Procedia Eng.* **2013**, *57*, 572–582. [[CrossRef](#)]
32. Prekajski, M.; Mirković, M.; Todorović, B.; Matković, A.; Marinović-Cincović, M.; Luković, J.; Matović, B. Ouzo Effect—New Simple Nanoemulsion Method for Synthesis of Strontium Hydroxyapatite Nanospheres. *J. Eur. Ceram. Soc.* **2016**, *36*, 1293–1298. [[CrossRef](#)]
33. Hadagalli, K.; Kumar, R.; Mandal, S.; Basu, B. Structural, Compositional and Spectral Investigation of Prawn Exoskeleton Nanocomposite: UV Protection from Mycosporine-like Amino Acids. *Mater. Chem. Phys.* **2020**, *249*, 123002. [[CrossRef](#)]
34. Tironi, A.; Trezza, M.A.; Irassar, E.F.; Scian, A.N. Thermal Treatment of Kaolin: Effect on the Pozzolanic Activity. *Procedia Mater. Sci.* **2012**, *1*, 343–350. [[CrossRef](#)]
35. Benkacem, S.; Boudeghdegh, K.; Zehani, F.; Hamidouche, M.; Belhocine, Y. Preparation, Microstructure Studies and Mechanical Properties of Glazes Ceramic Sanitary Ware Based on Kaolin. *Sci. Sinter.* **2021**, *53*, 209–221. [[CrossRef](#)]
36. Mgbemena, C.O.; Ibekwe, N.O.; Sukumar, R.; Menon, A.R.R. Characterization of Kaolin Intercalates of Oleochemicals Derived from Rubber Seed (*Hevea brasiliensis*) and Tea Seed (*Camelia sinensis*) Oils. *J. King Saud. Univ. Sci.* **2013**, *25*, 149–155. [[CrossRef](#)]
37. Amenta, E.; King, H.E.; Petermann, H.; Uskoković, V.; Tommasini, S.M.; Macica, C.M. Vibrational Spectroscopic Analysis of Hydroxyapatite in HYP Mice and Individuals with X-Linked Hypophosphatemia. *Ther. Adv. Chronic Dis.* **2018**, *9*, 268–281. [[CrossRef](#)] [[PubMed](#)]
38. Frost, R.L.; Thu Ha, T.; Kristof, J. FT-Raman Spectroscopy of the Lattice Region of Kaolinite and Its Intercalates. *Vib. Spectrosc.* **1997**, *13*, 175–186. [[CrossRef](#)]
39. Horváth, E.; Kristóf, J.; Frost, R.L. Vibrational Spectroscopy of Intercalated Kaolinites. Part I. *Appl. Spectrosc. Rev.* **2010**, *45*, 130–147. [[CrossRef](#)]
40. Peng, H.; Vaughan, J.; Vogrin, J. The Effect of Thermal Activation of Kaolinite on Its Dissolution and Re-Precipitation as Zeolites in Alkaline Aluminate Solution. *Appl. Clay Sci.* **2018**, *157*, 189–197. [[CrossRef](#)]
41. Garskaite, E.; Gross, K.-A.; Yang, S.-W.; Yang, T.C.-K.; Yang, J.-C.; Kareiva, A. Effect of Processing Conditions on the Crystallinity and Structure of Carbonated Calcium Hydroxyapatite (CHAp). *CrystEngComm* **2014**, *16*, 3950. [[CrossRef](#)]
42. Skinner, H.C.W.; Kittelberger, J.S.; Beebe, R.A. Thermal Instability in Synthetic Hydroxyapatites. *J. Phys. Chem.* **1975**, *79*, 2017–2019. [[CrossRef](#)]
43. Ondro, T.; Trník, A. Kinetic Behaviour of Thermal Transformations of Kaolinite. In Proceedings of the 23rd International Meeting of Thermophysics 2018, Smolenice, Slovakia, 7–9 November 2018; p. 020033.
44. Faqir, N.M.; Shawabkeh, R.; Al-Harathi, M.; Wahhab, H.A. Fabrication of Geopolymers from Untreated Kaolin Clay for Construction Purposes. *Geotech. Geol. Eng.* **2019**, *37*, 129–137. [[CrossRef](#)]
45. Li, X.; Ouyang, J.; Zhou, Y.; Yang, H. Assembling Strategy to Synthesize Palladium Modified Kaolin Nanocomposites with Different Morphologies. *Sci. Rep.* **2015**, *5*, 13763. [[CrossRef](#)] [[PubMed](#)]
46. Dwari, R.K.; Mishra, B.K. Evaluation of Flocculation Characteristics of Kaolinite Dispersion System Using Guar Gum: A Green Flocculant. *Int. J. Min. Sci. Technol.* **2019**, *29*, 745–755. [[CrossRef](#)]
47. Hadagalli, K.; Panda, A.K.; Mandal, S.; Basu, B. Faster Biomineralization and Tailored Mechanical Properties of Marine-Resource-Derived Hydroxyapatite Scaffolds with Tunable Interconnected Porous Architecture. *ACS Appl. Bio Mater.* **2019**, *2*, 2171–2184. [[CrossRef](#)] [[PubMed](#)]
48. Pan, Y.; Xiong, D. Study on Compressive Mechanical Properties of Nanohydroxyapatite Reinforced Poly(Vinyl Alcohol) Gel Composites as Biomaterial. *J. Mater. Sci. Mater. Med.* **2009**, *20*, 1291–1297. [[CrossRef](#)]
49. Sabree, I.; Gough, J.E.; Derby, B. Mechanical Properties of Porous Ceramic Scaffolds: Influence of Internal Dimensions. *Ceram. Int.* **2015**, *41*, 8425–8432. [[CrossRef](#)]
50. Yu, H.; Matthew, H.W.; Wooley, P.H.; Yang, S. Effect of Porosity and Pore Size on Microstructures and Mechanical Properties of Poly- ϵ -caprolactone-Hydroxyapatite Composites. *J. Biomed. Mater. Res. B Appl. Biomater.* **2008**, *86B*, 541–547. [[CrossRef](#)]

51. Akram, M.; Ahmed, R.; Shakir, I.; Ibrahim, W.A.W.; Hussain, R. Extracting Hydroxyapatite and Its Precursors from Natural Resources. *J. Mater. Sci.* **2014**, *49*, 1461–1475. [[CrossRef](#)]
52. Komalkrishna, H.; Jyoth, S.T.; Kundu, B.; Mandal, S. Low Temperature Development of Nano-Hydroxyapatite from Austromegabalanus Psittacus, Star Fish and Sea Urchin. *Mater. Today Proc.* **2017**, *4*, 11933–11938. [[CrossRef](#)]

Disclaimer/Publisher's Note: The statements, opinions and data contained in all publications are solely those of the individual author(s) and contributor(s) and not of MDPI and/or the editor(s). MDPI and/or the editor(s) disclaim responsibility for any injury to people or property resulting from any ideas, methods, instructions or products referred to in the content.